Perimeter growth of a branched structure: Application to crackle sounds in the lung

Adriano M. Alencar,[1,2,*] Sergey V. Buldyrev,[2] Arnab Majumdar,[2] H. Eugene Stanley,[2] and Béla Suki[1]

[1]*Department of Biomedical Engineering, Boston University, Boston, Massachusetts 02215, USA*
[2]*Center for Polymer Studies and Department of Physics, Boston University, Boston, Massachusetts 02215, USA*
(Received 25 February 2003; published 21 July 2003)

We study an invasion percolation process on Cayley trees and find that the dynamics of perimeter growth is strongly dependent on the nature of the invasion process, as well as on the underlying tree structure. We apply this process to model the inflation of the lung in the airway tree, where crackling sounds are generated when airways open. We define the perimeter as the interface between the closed and opened regions of the lung. In this context we find that the distribution of time intervals between consecutive openings is a power law with an exponent $\beta \approx 2$. We generalize the binary structure of the lung to a Cayley tree with a coordination number Z between 2 and 4. For $Z=4$, β remains close to 2, while for a chain, $Z=2$ and $\beta=1$, exactly. We also find a mean field solution of the model.

I. INTRODUCTION

There is much current interest in crackles; abrupt and discrete events triggered by small changes in the state of a given system [1]. Crackling behavior is found in a wide variety of systems including earthquakes [2], magnetic materials [3], crumpled elastic sheets [4], paper tearing [5], and mammalian lungs [6–10]. Usually, crackles span many orders of magnitude in loudness, amplitude, and the distribution of sizes follows a power law.

Pulmonary crackles are short, explosive, transient waves, which are among the many lung sounds generated in the airways of a diseased lung during breathing. They are characterized by a rapid initial pressure deflection, called a spike, followed by a short duration ringing. Crackles have long been used as a qualitative diagnostic tool, since their acoustic properties correlate with certain pulmonary dysfunctions [7,11–18]. The time series of crackle events are complex and two power laws have been discovered: one in the distribution of crackle sound amplitudes [10] and one in the time intervals between consecutive crackles [9]. However, much analysis of lung sound is based on empirical observations without solid theoretical basis.

The airway tree structure of the mammalian lung is binary and asymmetric [19–22]. The main function of the airway tree structure is to conduct air from the atmosphere to the gas exchange region, which is composed of more than 300 $\times 10^6$ alveoli or tiny, thin-membraned sacs. The internal surface of the lung is lined with a thin liquid film which can undergo a surface-tension-driven fluid-elastic instability, leading to airway closure by the formation of occluding liquid bridges [23,24]. Airway closure and reopening occur often in diseased lungs and are associated with the generation of respiratory crackles [7,25]. Studies of airway closure and opening indicate that during inflation, airways open in avalanches triggered by overcoming a hierarchy of critical opening threshold pressures along the airway tree [26–29]. Avalanche behavior is also present in chemical activities [30],

ferromagnetic materials [31,32], popping bubbles [33], and in others finite systems [34,35].

It is well established that the growth of colloid aggregates, flame fronts, and tumors occur mainly at the "active surface" [36,37], a concept also used to describe catalysis [38], polymerization, and percolation processes [39]. In particular, the problem of lung inflation can be modeled as an invasion percolation process on a branched structure [27,40]. In general, the active surface is defined as the perimeter where growth occurs. We define the active surface in the lung, or active perimeter, as the set of all closed branches connected to the root of the tree through an open pathway. During the growth of the active surface, acoustic energy is released as audible crackles [9].

Recently, we obtained a mean field solution for a model of the evolution of the active surface and the distribution of time intervals Δt between consecutive crackles in a *symmetric* Cayley tree. We assumed that the airway opening pressures are uniformly distributed [9,27]. Here, we explore the effects of *asymmetry* in the Cayley tree, coordination number Z, and generation-dependent thresholds on both the active surface and the distribution of Δt. We find that the active surface is sensitive to the asymmetry of the tree structure, Z, and generation dependence of the airway opening threshold pressure. However, the distribution of Δt is insensitive to changes in Z for $Z>2$.

This paper is organized in the following way. We briefly describe the experimental procedure in Sec. II. In Sec. III, we describe the dynamic model with the parameters used in this paper. In Sec. IV, we show the numerical simulations. In Sec. V, we analytically solve the model and in Sec. VI, we present a short discussion.

II. EXPERIMENTAL DATA

A time series of sound amplitudes was recorded in the main bronchus of dog lung lobes during inflation from the collapsed state to the total lobe capacity in a time t_{max} $=120$ s [10]. At the beginning of inflation, the sound pressure time series displays a set of discrete crackles [see Fig. 1(a)]. With advancing inflation, massive airway opening gen-

*Electronic address: adriano@bu.edu
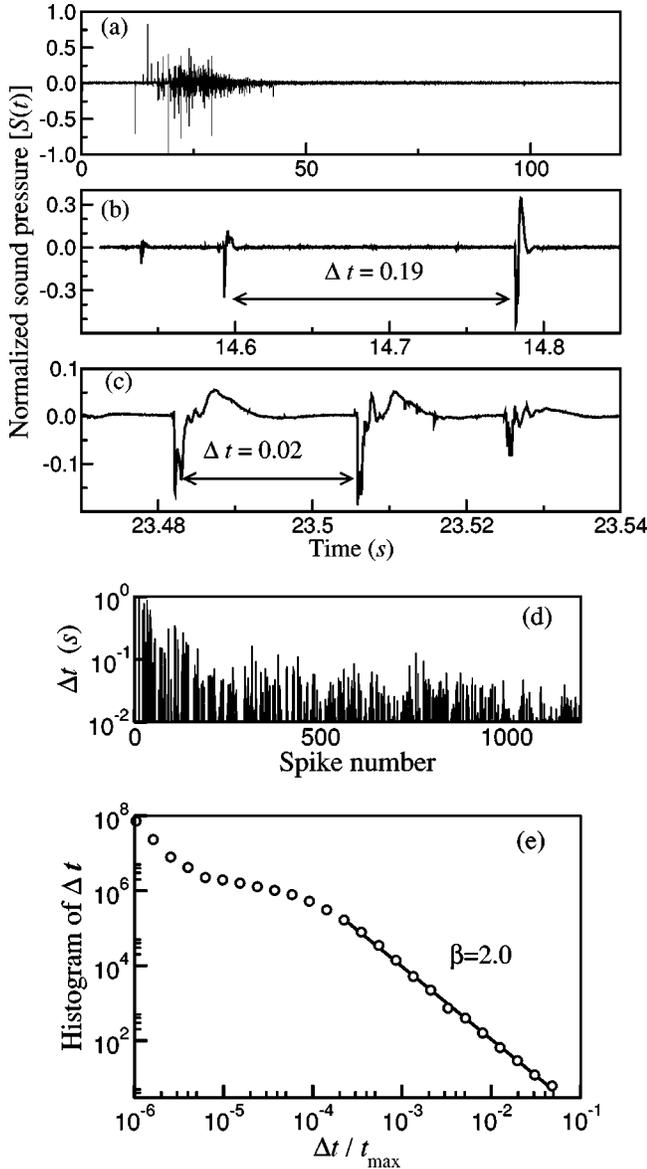
FIG. 1. Experimental data. (a) The continuous line is the time series of sound pressure $S(t)$ during the first inflation of a dog lung lobe from the collapsed state, recorded at a rate of 22 050 Hz. (b) Magnified segment of $S(t)$ with consecutive spikes. The interspike interval $\Delta t \approx 0.2$ s of this segment corresponds to the time difference between two spikes; (c) another segment from (a) with $\Delta t \approx 0.02$ s; (d) the sequence of time intervals Δt from (a); and (e) the histogram of interspike intervals for 12 different inflations [9].

erates dense and overlapping wave packets [see Fig. 1(a)]. The envelope of the time series gradually decreases with inflation, indicating first the generation of coarse crackles, then later of fine crackles [11]. To characterize the statistical features of the crackles, we develop a moving window algorithm that measures the spike size in the time series and the time delay Δt between two consecutive spikes [see Figs. 1(b) and 1(c)]. An example of the Δt series is shown in Fig. 1(d). The distribution $\Pi(\Delta t)$ of Δt [Fig. 1(e)] shows one pronounced regime of power law behavior, $\Pi(\Delta t) = \Delta t^{-\beta}$, with $\beta = 2.0$. The large Δt regime is related to the dynamics of

distinct avalanches and the small Δt regime is related to the dynamics of crackles within a single avalanche [9]. The dynamics of distinct avalanches play an important role in the recruitment of closed regions of the lung and will be the main focus of this paper.

III. A DYNAMIC MODEL OF CRACKLE GENERATION

To understand the scaling behavior of Δt, we develop a dynamic invasion percolation model which considers the time required for an airway to open and the avalanche to propagate through an M-generation airway tree. For simplicity, we first treat a symmetric tree structure, then generalize to an asymmetric tree.

In Sec. III A, we mathematically model the lung as a Cayley tree with a coordination number Z. When the lung is degassed, airways collapse, closing most pathways downstream. To mimic the process of reopening, we assign the opening threshold pressure P_{th} as a parameter to each airway (Sec. III B). If the airway is connected through an open pathway to the root of the tree and the external pressure P_E reaches P_{th}, the airway opens and a crackle is locally generated. In Sec. III C, we describe the timing related to the inflation process.

A. Airway tree structure

Like botanical trees and rivers, the airway tree structure is binary and asymmetric. A structure is called a binary tree if each node has three connections ($Z=3$): a parent branch and two daughters. $Z=2$ defines a chain and $Z=4$ is a tree that trifurcates at each node [60].

In this model, each branch is labeled (i,j), where i is the generation number from the root of the tree ($i = 1, 2, \ldots, M$) and, for a generic tree, $j \in [0, (Z-1)^i - 1]$ is used to distinguish between branches of the same generation [61]. The root of the tree is labeled $(0,0)$.

B. Airway closure and opening

When the lung deflates to very low volumes, many peripheral airways close by forming a liquid bridge between the collapsed airway walls [23,24,41–43]. Each branch (i,j) is closed at the beginning of the inflation ($t=0$). Experiments and models indicate that a critical opening threshold pressure $P_{i,j}$ can characterize the opening of a single airway [44,45]. Thus, all branches (i,j) are assigned a random $P_{i,j}$ uniformly distributed between 0 and P_{max}. The simplest model, when $P_{i,j}$ is uniformly distributed independent of the generation number, or airway diameter, has been explored in previous studies [9,10,26,29,46,47]. Imposing a generation dependence on $P_{i,j}$ is not straightforward, since few experimental data exist on how airway generation in the lung affects the opening threshold pressures. However, theoretical studies suggest that the pressure threshold depends on several physiological parameters such as surfactant, surface tension, liquid layer thickness, and airway elastic properties [48–50].

The two major factors contributing to $P_{i,j}$ are the diameter of the airways and the surface tension of the obstructing

liquid. The diameter of the airway decreases from the root of the tree to the air sacs and numerical values are known [21,51]. On the other hand, surfactant is secreted by lung cells lining the bottom portion of the tree and the air sacs. Surfactant diffuses toward the root of the tree and, thus, the concentration of surfactant is higher at the bottom than at the top [52]. Since the surfactant reduces the surface tension of the obstructing liquid, the surface tension at the bottom of the tree is smaller than at the top. Direct experimental evidence of the opening threshold in a lung tree has been observed, showing that the opening threshold is inversely dependent on the diameter d and proportional to the surface tension γ,

$$P(d) = \frac{\mathcal{C}\gamma}{d}, \tag{1}$$

where $\mathcal{C}$ is a constant [45]. The two competing factors γ and d have been used as an argument for the use of generation-independent random $P_{i,j}$, where the randomness comes from the opposite nature of both contributions. We introduce generation dependence of $P_{i,j}$ by adding a deterministic term, which shifts the mean of the distribution of $P_{i,j}$. Thus, assuming that $P_{i,j}$ is not deterministic, we can add a random term and write

$$P_{i,M} = \frac{\mathcal{C}\gamma_{i,M}}{d_i} + \eta, \tag{2}$$

where the surface tension $\gamma_{i,M}$ is a function of the surfactant concentration, that is, a function of the generation number i and the maximum number of generations in the tree M, and η is the random term.

C. The process of inflation

Inflation is simulated by applying an external pressure $P_E(t)$ at the root of the tree and uniformly increasing $P_E(t) = Kt$ in small increments, where $K = P_{max}/t_{max}$ is a constant inflation rate. In this model, we rescale both time and pressure so that $P_{max} = 1$ and $t_{max} = 1$, making $K = 1$.

Since an airway opens when the pressure in its parent exceeds its critical opening threshold, the airway (0,0) opens when $P_E = P_{0,0}$ at $t_{0,0} = P_{0,0}$, where $t_{0,0}$ is now the time associated with the opening of the root. Next, the daughter airways are checked; one, or two, or all will open if $P_E \geq P_{1,j}$, where j distinguishes different airways at the same generation. This opening process is then continued sequentially down the tree until no airway connected to the root is found with $P_{i,j} \leq P_E$. Note that the opening of a single branch can lead to openings of other branches which have $P_{i,j} < P_E$, defining an avalanche in which many airways open in a cascade (Fig. 2). The opening of an airway also generates a crackle sound locally, which we model as an acoustic spike.

The opening of the first segment or root of an avalanche, airway (i,j), occurs at time

$$t_{i,j} = P_{i,j}, \tag{3}$$
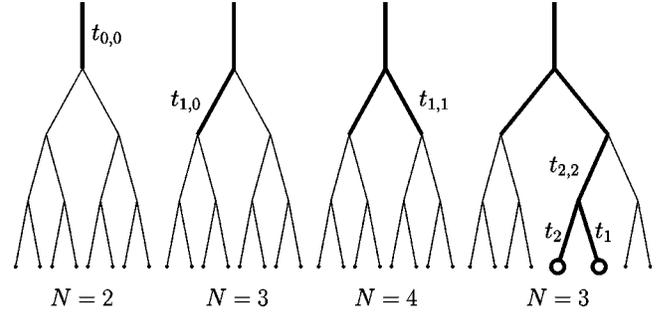
FIG. 2. Diagrams describing avalanche timing for a tree with $Z = 3$. Initially, just the root is open and the time for that event is $t_{0,0}$. The number of segments on the active surface that are closed is $N = 2$. The pressure increases and the left daughter opens at $t_{1,0}$ and now $N = 3$. Following a new increase of pressure, the right daughter of the root opens at $t_{1,1}$ and $N = 4$. Next, the left daughter opens at $t_{2,2}$ which triggers an avalanche, where each segment of this avalanche has a time delay (t_1 and t_2) with respect to $t_{2,2}$. When the avalanche stops, $N = 3$.

since P_E increases linearly with time. Thus, the time difference between two consecutive avalanches is

$$\Delta t = \Delta P, \tag{4}$$

or the pressure difference between P_E values that trigger two consecutive avalanches. However, the time associated with events inside the same avalanche is independent of the inflation time; it will be related to the time required for a pressure wave to travel from an opening to reach the next daughter airway.

IV. NUMERICAL SIMULATIONS

To understand the contribution of the interavalanche time intervals to the power law distribution of Δt, we assume that the time required to open all segments within an avalanche is negligible compared to interavalanche timings. Thus, all crackles from the same avalanche arrive simultaneously at the root, and only interavalanche time intervals are present in this study. We divide the numerical simulations in three parts. First, we study crackles in a binary tree ($Z = 3$) and simulate the effect of different pressure threshold distributions (Sec. IV A). Next, we study the effect of asymmetry of the tree structure for a binary tree (Sec. IV B). Then, to study the effect of branching, we simulate crackles in a chain ($Z = 2$) and a tree with $Z = 4$ (Sec. IV C).

A. Binary tree ($Z = 3$) with different $P_{i,j}$ distributions

We numerically simulate the generation of crackle sounds in a symmetric binary tree using two rules: rule (i) the $P_{i,j}$ are generation independent and are completely random, having no deterministic part, Sec. IV A 1; rule (ii) the $P_{i,j}$ are generation dependent and the dependence can be either weak or strong, Sec. IV A 2. In all numerical simulations for binary trees, the diameter of the airways are assigned according to Ref. [51], with values of d between 1, for the root of the tree, and 0.034, for the smallest airways in a tree with 15
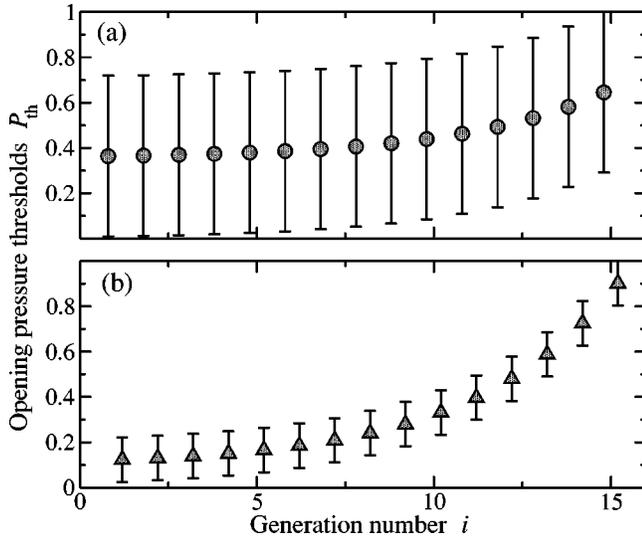
FIG. 3. Opening threshold pressure $P_{i,j}$ used for the weak and strong generation dependence. (a) Circles are the mean of P_{th} for $\mathcal{C}=0.01$ and (b) triangles are for $\mathcal{C}=0.1$ in Eq. (2). The error bar denotes the maximum and minimum value.

generations. For the purpose of these simulations, we select $\mathcal{C}=1$, and the random term η in Eq. (2) is distributed uniformly between 0 and 1. For all models, the opening threshold pressures $P_{i,j}$ are normalized so that the maximum value $\max(P_{i,j})=1$. Figure 3 shows the normalized maximum value of $P_{i,j}$ as a function of the diameter for models B and C.

1. Generation independent, uniform distributions of $P_{i,j}$

We obtain generation-independent opening threshold pressures $P_{i,j}$ when we neglect the first term of Eq. (2) by considering $\mathcal{C}=0$. Thus, after normalization, only the random term η will contribute to $P_{i,j}$. We calculate the dynamic active surface of the interface between the closed and open regions of the lung for 15 generations [Fig. 4(a)]. From numerical simulations in a symmetric tree, using M up to 20 generations, we obtain a single power law with exponent $\beta =2.1$ for the distribution of the time intervals between consecutive avalanches [see Fig. 4(d)]. The active surface from individual simulations shows a large deviation around the average behavior and its maximum value around 1000 airways is small compared to the total number of airways, in this case, $M=15$ having 32 769 airways [see Fig. 4(a)].

2. Generation dependent $P_{i,j}$

We obtain a weak dependence of the opening threshold pressure $P_{i,j}$ on the generation number by assuming that the concentration of lung surfactant inside the lung is constant, i.e., the surface tension $\gamma_{i,M}$ is independent of the generation. Note that in this case, the first term of Eq. (2) makes a small contribution to the opening threshold pressure (Fig. 3). The active surface significantly changes compared to the generation-independent case [Fig. 4(b)]. The maximum value of the active surface size is larger. This behavior is because all avalanches tend to stop early, reducing the probability of reaching the alveoli and hence reducing the active surface
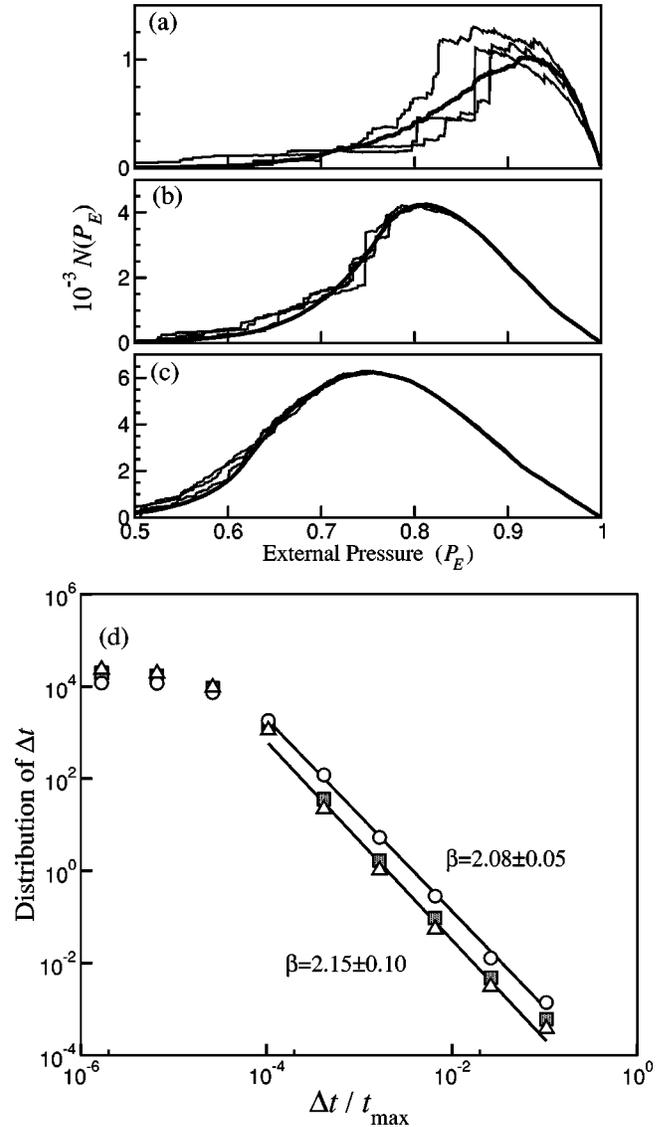
FIG. 4. Plot of the number of active segments N along the active surface as a function of the external pressure P_E for the numerical simulations of the generation independent, weak and strong generation dependence. For these simulations, we used a symmetric 15-generation tree. The thin lines are independent simulations and the thick lines are averages over 1000 simulations: (a) generation independent, (b) weak generation dependence, and (c) strong generation dependence. (d) Distribution of time intervals between consecutive crackles in a tree with 15 generations for three different types of generation dependence. Circles represents generation independent, squares weak generation dependence, and triangles strong generation dependence.

size. The deviation between individual simulations and the average behavior is smaller than in the generation-independent case because $P_{i,j}$ is more deterministic. However, the distribution of time intervals between consecutive crackles does not change [Fig. 4(d)].

We increase the generation dependence of the $P_{i,j}$ by setting $\gamma_{i,M}=0.02$ in Eq. (2). Now, the effect of the surface tension and the dependence of the diameter on the opening pressure threshold is twice as strong as in the weak genera-

tion dependence (Fig. 3). In this simulation, the maximum value of the active surface is even higher than in the weak generation dependence and the deviations between different simulations are even smaller [Fig. 4(c)]. Again, the distribution of Δt is almost unaffected, indicating that the power law behavior of Δt is weakly related to the distribution of $P_{i,j}$.

One important result of these simulations is that the dynamic properties of the active surface are dependent on the type of opening threshold pressures used. Comparing the active surfaces from the generation-independent and generation-dependent models, one can see that the maximum size N of the active surface increases and its position shifts from $P_E = 0.9$ to 0.7 when we increase the generation dependence of $P_{i,j}$. This behavior is expected, since the sizes of the avalanches tend to decrease when the opening threshold pressure is more dependent on the generation. On the other hand, the statistical behavior of the time intervals between consecutive crackles remains almost unchanged for all generation dependent $P_{i,j}$ [Fig. 4(d)]. Previously, we had shown that when $P_{i,j}$ is uniformly distributed, the power law distribution of the time interval between consecutive crackles is due to the hierarchical tree structure [9]. The present results further confirm that the scaling originates from the tree structure. Another point is that the active surface decreases only when avalanches or single openings propagate to the alveoli without leaving any closed branches in their path. Figure 4(b) shows that at 0.8 $P_{max} \approx 2^{12}$, branches are on the active surface, as if all branches at generation 13 were closed and all branches up to generation 12 were open in a 15-generation tree.

B. Asymmetric binary tree structure (Z=3)

It is known that the mammalian lung is asymmetric with the asymmetry varying from species to species [21,53]. There are several different ways to generate an asymmetric tree structure that is similar to the lung. We use a flow division model which generates realistic tree structures [51]. In this model, we control the degree of asymmetry using a flow division parameter r, which is the ratio of the flow entering the left daughter branch from the parent. A terminal air sac is placed at the end of all airways, which have a flow smaller than a given threshold. We can increase the size of the tree by reducing this threshold [51]. For a symmetric tree at each node, half of the flow goes to one daughter and the other half goes to the other daughter, thus $r = 0.5$. If r is different from 0.5, more flow goes to one side or to the other side, leading to asymmetry. We use this model to study the effect of asymmetry on the active surface.

We carried out numerical simulations for two values of r, $r = 0.25$ and $r = 0.15$, and compared with the symmetric tree $r = 0.5$. Figure 5 shows the active surface of three independent simulations and the distribution of time intervals for 1000 simulations. Again, the asymmetry changes the active surface but not the distribution of time intervals.

C. Tree structures with Z=2 and Z=4

In order to study the effect of different branching of the tree structure on the active surface and the distribution of Δt,
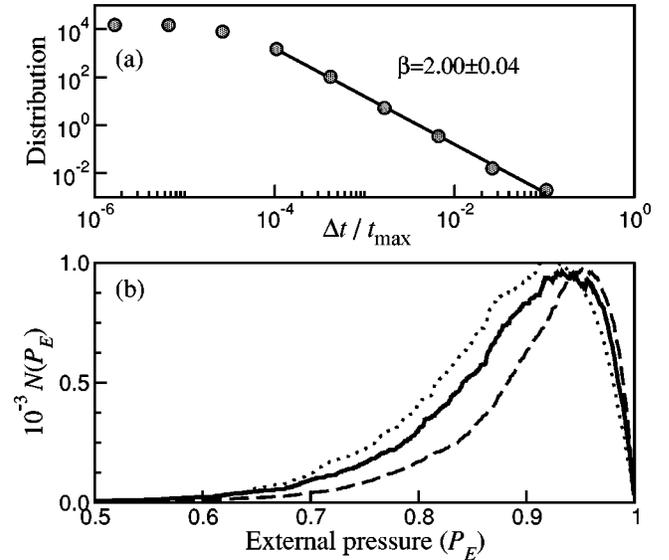
FIG. 5. Numerical simulations using an asymmetric tree structure. (a) Time interval between consecutive crackles for 1000 independent simulations in a 15-generation tree. This result is independent of r in the range $0.25 \leq r \leq 0.5$; (b) plot of the number of active segments N as a function of the external pressure P_E (dots) symmetric tree, $r = 0.5$ (line) asymmetric tree with $r = 0.25$, and (dashed) asymmetric tree with $r = 0.15$.

we first study the case of a chain $Z = 2$, then a tree with $Z = 4$ and then compare the results with simulations on a binary tree. For simplicity, in this section all simulations use generation independent $P_{i,j}$.

1. Chainlike structure, Z=2

A chain does not have a shape similar to the mammalian lung. The active surface of a chain with random closures is always one branch. However, we can find the time interval between consecutive avalanches. Here, the generation number is the total number of branches in the chain (to be consistent with the previous sections we use $M = 2^{15}$ branches). We assume that all segments are closed with uniformly distributed random thresholds. In Fig. 6, we show the results for the distribution of time intervals between consecutive events. Note that now the distribution of time intervals dramatically changes and $\beta = 1$.

2. Tree structure with Z=4

A tree with coordinate number $Z = 4$ is similar to some botanical trees. In Fig. 7, we show the results for the time interval distribution between consecutive events. Note that now the distribution of time intervals is again $\beta \approx 2$, and the functional form of the active surface is almost unchanged compared with $Z = 3$. The major difference is a magnification in the $N(P_E)$ axis due to the increase of the number of segments in the tree.

V. ANALYTIC CALCULATION

A. Chain model

A chain is a Cayley tree with $Z = 2$ and M segments, or airways. At each node we assign a random opening threshold
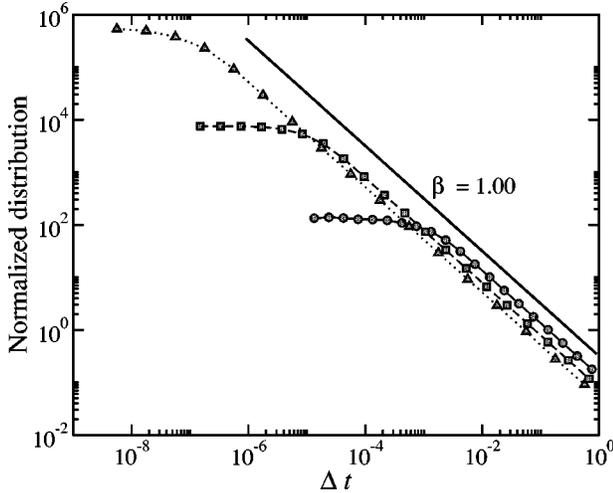
FIG. 6. Distribution of numerical simulations of Δt for a chain $Z=2$. Circles show the distribution for a chain with $M=10^{13}$ segments, square for $M=10^{15}$, and triangle for $M=10^{17}$. The thick line is a curve with exponent $\beta=1.00$.

pressure. Note that for a chain, the perimeter is always a single segment. An airway i is the perimeter only when all airways before it has $P_j < P_E$, for $0 \leq j < i$, and $P_i > P_E$. When a branch opens, all following branches also open in an avalanche process until the avalanche process reaches the end of the chain or an airway i with $P_i > P_E$, which becomes the new perimeter.

In order to find the distribution of time intervals between consecutive avalanches, we recognize that the M segments of the chain open in N subgroups of segments, each subgroup constituting an avalanche. In each avalanche, the first seg-
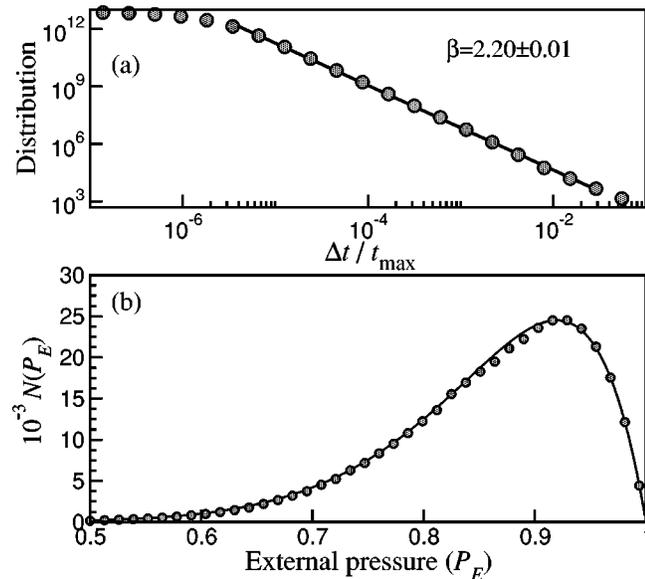
FIG. 7. Numerical simulation of the time interval between consecutive crackles for 300 independent simulations in a tree with $Z=4$ and $M=12$. (a) Distribution of time intervals between consecutive crackles; (b) plot of the number of active segments N as a function of the external pressure P_E in the simulations (circles) and prediction from the analytical formulation Eq. (33) (line).

ment has the largest threshold pressure. The threshold pressures of the first segments of the avalanches are in a strictly increasing order. Thus, the probability of partitioning the M segments of the chain into N distinct avalanches is given by the Stirling numbers of the first kind, $S(N,M)$, which gives the probability of partitioning M segments into N cycles [54,55]. In each cycle, the first segment must have the largest P_{th}, and the rest can be placed arbitrarily, with the first segments of the cycles placed in an ascending order. The order of the segments in the cycles uniquely defines a configuration of avalanches.

The Stirling numbers $S(N,M)$ are defined as [54]

$$S(N,M) = \frac{1}{M} \sum_{k=N-1}^{M-1} S(N-1,\ k), \tag{5}$$

with $S(1,\ k)=1/k$. The generating function $g_M(x)$ for these probabilities is given by

$$g_M(x) = \frac{x(x+1)(x+2)\cdots(x+M-1)}{M!} = \sum_{k=1}^{M} S(k,M)x^k. \tag{6}$$

For $M \to \infty$, the Stirling numbers converge to a Gaussian distribution with mean [56]

$$\langle N(M) \rangle = g_N'(x)|_{x=1} = \sum_{N=1}^{M} \frac{1}{N} \approx \ln M + c \tag{7}$$

and variance

$$\sigma^2 = g''(x)|_{x=1} + g'(x)|_{x=1} - g'(x)^2|_{x=1}$$

$$= \sum_{N=1}^{M} \frac{1}{N} - \sum_{N=1}^{M} \frac{1}{N^2} \approx \ln M + c - \frac{\pi^2}{6}, \tag{8}$$

where $c = 0.577\ldots$ is the Euler number. This result gives the average number of avalanches $\langle N(M) \rangle$ in a chain with M segments, or in this case, generations.

The next step is to find the probability $\Pi_N(\Delta t)$ of finding a time interval Δt in a sequence of N avalanches. We will derive the distribution of the interavalanche time intervals $\Delta t_n = P_n - P_{n-1}$ [see Eq. (4)], where P_n is the opening threshold pressure of the nth avalanche. If the opening threshold pressure of the root $P_0 = 0$, the distribution of the first interavalanche time interval Δt_1 is uniform in the interval $[0,1]$,

$$\pi_1(\Delta t_1) = \begin{cases} 1 & \text{if } 0 \leq \Delta t_1 \leq 1 \\ 0 & \text{otherwise.} \end{cases} \tag{9}$$

To calculate the distribution of Δt_n, we first define the quantity $x_n = 1 - P_n$ (see Fig. 8). Thus,

$$\Delta t_n = x_{n-1} - x_n. \tag{10}$$

For a given x_{n-1}, the value of x_n is uniformly distributed between 0 and x_{n-1}. Thus, the conditional probability
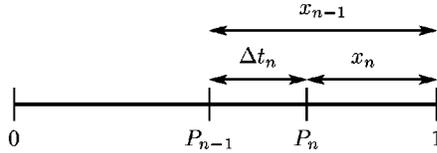
FIG. 8. Schematic representation of the opening process in a chain and the illustration of Eq. (10).

$$p(x_n|x_{n-1}) = \begin{cases} 1/x_{n-1} & \text{if } 0 \le x_n \le x_{n-1} \\ 0 & \text{otherwise.} \end{cases} \quad (11)$$

Using Eq. (10), we can calculate the conditional probability

$$p(\Delta t_n|x_{n-1}) = \begin{cases} 1/x_{n-1} & \text{if } 0 \le \Delta t_n \le x_{n-1} \\ 0 & \text{otherwise.} \end{cases} \quad (12)$$

The distribution of the nth interavalanche time interval $\pi_n(\Delta t_n)$ can be defined as the convolution

$$\pi_n(\Delta t_n) = \int_0^1 p(\Delta t_n|x_{n-1}) \tilde{\pi}_{n-1}(x_{n-1}) dx_{n-1}, \quad (13)$$

where $\tilde{\pi}_n$ is the distribution of the quantity x_n, which can be similarly expressed as

$$\tilde{\pi}_n(x_n) = \int_0^1 p(x_n|x_{n-1}) \tilde{\pi}_{n-1}(x_{n-1}) dx_{n-1}. \quad (14)$$

Since the expressions in Eqs. (12) and (13) are identical to those in Eqs. (11) and (14), respectively, the distributions $\tilde{\pi}_n$ and π_n are given by identical functions. We can thus replace the variable x_{n-1} inside the integral in Eq. (13) with Δt_{n-1} and the corresponding distribution $\tilde{\pi}_{n-1}$ with π_{n-1}. Thus, using Eq. (12) we can write the distribution of the nth time interval Δt_n in terms of the distribution of the $(n-1)$th time interval Δt_{n-1} as

$$\pi_n(\Delta t_n) = \int_{\Delta t_n}^1 \frac{\pi_{n-1}(\Delta t_{n-1})}{\Delta t_{n-1}} d\Delta t_{n-1}. \quad (15)$$

Thus, using Eqs. (9) and (15) we can write the hierarchy of distributions

$$\pi_2(\Delta t_2) = \int_{\Delta t_2}^1 \frac{1}{\Delta t_1} d\Delta t_1 = -\ln(\Delta t_2)$$

$$\vdots$$

$$\pi_N(\Delta t_N) = \int_{\Delta t_N}^1 \frac{\ln^{N-2}(\Delta t_{N-1})(-1)^{N-2}}{\Delta t_{N-1}(N-2)!} d\Delta t_{N-1}$$

$$= \frac{\ln^{N-1}(\Delta t_N)(-1)^{N-1}}{(N-1)!}. \quad (16)$$

Suppose we have exactly N avalanches in our chain. The distribution of intervals Δt for all N avalanches is thus
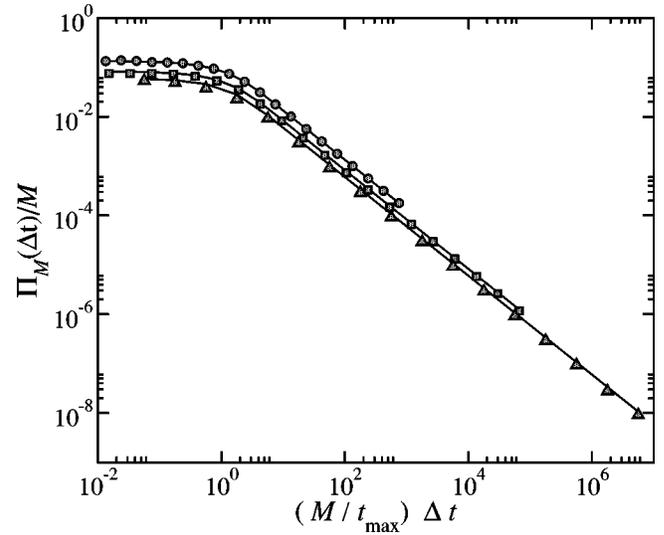
FIG. 9. Collapsed distribution of Δt for a chain with 10^3 segments (circles); $M = 10^5$ (squares); and $M = 10^7$ (triangles). The lines are the analytical plots of Eq. (20).

$$\Pi_N(\Delta t) = \frac{1}{N} \sum_{k=0}^{N-1} \frac{\ln^k(\Delta t)}{k!} (-1)^k. \quad (17)$$

If $\Delta t \gg 1/N$,

$$\Pi_N(\Delta t) \approx \frac{1}{N\Delta t}. \quad (18)$$

In the case of fixed number of generations M, we substitute the number of avalanches N in Eq. (18) with the expression for $\langle N(M) \rangle$ given by Eq. (7),

$$\Pi_N(\Delta t) \approx \frac{1}{\Delta t(\ln M + c)}. \quad (19)$$

However, to find an interval $\Delta t \le 1/\langle N \rangle$, we can use the simplest model in queuing theory. This model is used for arrivals into a queue system, assuming that the probability of an arrival in a small interval of time depends only on the size of the interval, not on any history of the process [57]. Thus, the probability of having $\Delta t \le 1/\langle N \rangle$ for M thresholds is given by the Poisson distribution $1 - \exp(-\Delta t M)$. We can conjecture that the probability distribution must be well approximated by the product

$$\Pi_M(\Delta t) = \frac{1 - \exp(-\Delta t M)}{\Delta t(\ln M + c)}. \quad (20)$$

Thus, the cutoff of the distribution occurs at $\Delta t = 1/M$ and the three curves from Fig. 6 can be collapsed into a single master curve [see Fig. 9]. We test our conjecture by plotting $\Pi_M(\Delta t/M)/M$ with the simulations for $M = 10^3$, 10^5, and 10^7 (see Fig. 9).
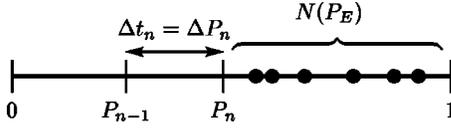
FIG. 10. Schematic representation of the inflation. The bullets in the pressure axis indicate the $P_{i,j}$ for all airways on the active surface. $N(P_E)$ is the number of airways on the active surface at pressure P_E. When P_E increases and reaches the segment with smallest P_{th} on the active surface, that airway opens, and $Z-1$ new values of $P_{i,j}$ drop in the pressure axis. If the new values of $P_{i,j}$ $\leqslant P_E$, these airways open in avalanche, otherwise $P_{i,j} > P_E$ and the airway will be on the active surface.

B. Symmetric tree, $Z>2$

First, we consider the case where $P_{i,j}$ is uniformly distributed. At $t=0$, the root of the tree is closed and the probability of it being open is equal to the external pressure $P_E(0)$ $=0$. During the time interval Δt_n between two consecutive avalanches n and $n+1$, the inflation is blocked by the closed airways on the active surface. The closed airways on the active surface have opening threshold pressures $P_{i,j}$ uniformly distributed between $P_E(n)$ and 1, where $P_E(n)$ is the external pressure that has produced the nth avalanche. The number of closed airways $N(P_E)$ defines the size of the active perimeter at each external pressure P_E. The next avalanche takes place when P_E becomes equal to the smallest $P_{i,j}$ on the active surface (see Fig. 10),

$$P_E(n+1) = \min_{N(P_E)} \{P_{i,j}\}. \tag{21}$$

Thus, the interavalanche time interval Δt_n is defined by

$$\Delta t_n = \Delta P_n = \min_{N(P_E)} \{P_{i,j} - P_E(n)\}, \tag{22}$$

where the minimum is taken over all $N(P_E)$ closed airways on the active surface. Note that Δt is the difference between the minimum opening threshold pressure among the N segments on the active surface and the external pressure. Since each of the N segments has opening threshold pressures uniformly distributed between P_E and 1, the average value of Δt is given by $\overline{\Delta t} = (1-P_E)/N$.

In order to derive the distribution for Δt, we first find the probability of having no openings between P_E and P_E $+\Delta P$. Since the opening threshold pressures $P_{i,j}$ are uniformly distributed and consist of independent random variables, this probability is given by

$$\text{Prob}(\min\{P_{i,j}\} > P_E + \Delta P) = \left(1 - \frac{\Delta P}{1-P_E}\right)^N. \tag{23}$$

The probability distribution of ΔP (or Δt) is then given by differentiating Eq. (23) with respect to ΔP. This gives us

$$\Pi(\Delta t) = \frac{N}{1-P_E}\left(1 - \frac{\Delta t}{1-P_E}\right)^{N-1}.$$

If N is large enough, then

$$\Pi(\Delta t) \approx \frac{1}{\overline{\Delta t}}\left(1 - (N-1)\frac{\Delta t}{1-P_E}\right),$$

which can be approximated by

$$\Pi_n(\Delta t_n) \approx \frac{1}{\overline{\Delta t}_n} e^{-\Delta t_n / \overline{\Delta t}_n}, \tag{24}$$

which is the negative exponential distribution [58,59] with a mean value of

$$\overline{\Delta t}_n = \frac{1-P_E}{N(P_E)}. \tag{25}$$

The distribution of Δt during the entire inflation is, thus, the sum of the exponential distributions corresponding to all n $=1,2,\ldots,n_{\max}$ avalanches, where $n_{\max}$ is the total number of avalanches

$$\Pi(\Delta t) = \frac{1}{n_{\max}} \sum_{n=1}^{n_{\max}} \Pi_n(\Delta t_n). \tag{26}$$

To evaluate this sum, we express it in terms of P_E. For each realization of opening threshold pressures, the variables $N(P_E)$ and $\overline{\Delta t}_n$ are step functions of P_E. Since our goal is to find the distribution of Δt for all realizations of disorder, we will replace $N(P_E)$ and $\overline{\Delta t}_n$ by their averages over many realizations, denoted as $\langle \cdots \rangle$. For clarity, we introduce a new notation

$$\tau(P_E) \equiv \langle \overline{\Delta t}_n \rangle = \frac{1-P_E}{\langle N(P_E) \rangle}. \tag{27}$$

Accordingly, we will replace $\Delta P_n \equiv P_E(n+1) - P_E(n)$ by $\tau(P_E)$. Taking Eq. (24) into account, we approximate the sum in Eq. (26) by an integral from $P_E=0$ to $P_E=1$, corresponding to the summation from $n=1$ to $n=n_{\max}$

$$\Pi(\Delta t) \equiv \left(\frac{1}{n_{\max}}\right) \sum_{n=1}^{n_{\max}} \frac{\Pi_n(\Delta t_n)}{\Delta P_n} \Delta P_n$$

$$\approx \left(\frac{1}{n_{\max}}\right) \int_0^1 \frac{e^{-\Delta t/\tau(P_E)}}{\tau^2(P_E)} dP_E. \tag{28}$$

In order to calculate $\Pi(\Delta t)$, we need to find an explicit expression for $\langle N(P_E) \rangle$, since it is involved in Eq. (28) because of Eq. (27). For simplicity we consider a binary tree with $Z=3$. Suppose that on an average, the generation i contains L_i open branches connected with $2L_i$ branches at the next generation, which can be either open or closed. The average number of open branches at generation $(i+1)$ is L_{i+1}. Since the distribution of $P_{i,j}$ is uniform between 0 and 1, the fraction of open branches is equal to P_E. Hence, the number of opened branches in the $(i+1)$th generation is $L_{i+1} = 2P_E L_i$. This recursion relation has a solution

$$L_i = (2P_E)^i. \tag{29}$$
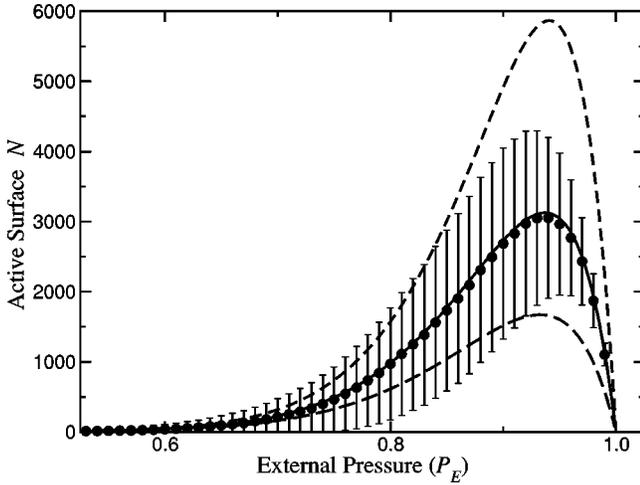
FIG. 11. Plot of the active surface. From the numerical model $M=17$, circles are the average N after 1000 simulations, and the error bar is the standard deviation. Lines are the analytical model for $M=16$-, 17-, and 18-generations trees from the bottom to the top, respectively. Note that at $M=17$, the numerical and the analytical model merge.

The number of closed branches connected to the root through open branches at generation $i+1$ is given by $N_{i+1}=2L_i-L_{i+1}$, making

$$N_{i+1}=2(1-P_E)(2P_E)^i. \qquad (30)$$

Note that Eq. (29) and, consequently, Eq. (30) is valid only if the root is open. An M generations tree with the root open is identical to a system composed of two $(M-1)$-generations trees with the roots closed. Thus, we divide Eq. (30) by two and increase by one generation. Now,

$$N_i=(1-P_E)(2P_E)^{(i-1)}. \qquad (31)$$

Thus,

$$\langle N(P_E)\rangle=\sum_{i=1}^{M} N_i=\frac{(2P_E)^M-1}{2P_E-1}(1-P_E). \qquad (32)$$

Figure 11 compares Eq. (32) with three different realizations of the numerical model for trees with $M=16$, 17, and 18.

We can generalize Eq. (32) for the case of a tree with a given coordination number Z, replacing Eq. (29) by $L_i=[(Z-1)P_E]^i$, and we get

$$\langle N(P_E)\rangle=\sum_{i=1}^{M} N_i=\frac{[(Z-1)P_E]^M-1}{(Z-1)P_E-1}(1-P_E). \qquad (33)$$

Substituting $\langle N(P_E)\rangle$ from Eq. (33) into Eq. (27), we obtain

$$\tau(P_E)=\frac{(Z-1)P_E-1}{[(Z-1)P_E]^M-1}. \qquad (34)$$

Finally, substituting Eq. (34) into Eq. (28), we obtain the explicit form for the distribution. The normalization constant n_{max} can be calculated as
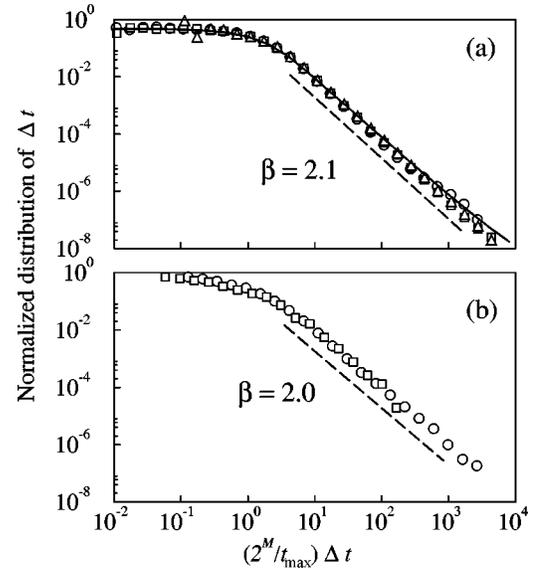
FIG. 12. Data collapse of the distributions normalized with $2^M/t_{max}$. (a) Numerical simulations for binary trees ($Z=3$) with $M=12$ generations (circles), $M=16$ generations (squares), and $M=20$ generations (triangles). The solid line represents Eq. (28) and the dashed line represents the best fit exponent for the numerical simulation with $M=20$. (b) Experimental data for the threshold of 1%, scaled with $M=14$ (circles) and for the threshold of 8%, scaled with $M=10$ (squares). The dashed line represents the best fit exponent for the data with the threshold of 1%.

$$n_{max}=\int_0^1 dP_E/\tau(P_E)\approx(Z-1)^M/M. \qquad (35)$$

For large M, the scaling properties of the integral in Eq. (28) can be estimated by the saddle point approximation: For $\Delta t\ll(Z-1)^{-M}$, we have a uniform distribution

$$\Pi(\Delta t)\approx(Z-1)^{M-1}. \qquad (36)$$

This equation gives us an interpretation of the plateau region of the experimental distribution of Δt. For $1/(Z-1)^M\ll\Delta t\ll1/M$, we have a power law decay

$$\Pi(\Delta t)\approx(Z-1)^{-M+1}\Delta t^{-2-1/M}. \qquad (37)$$

This equation gives us a mean field interpretation of the exponent $\beta\approx2$ from the experimental distribution of Δt for $Z=3$. The approximations we have used affect only the finite size correction of β, which is of the order of $1/M$.

Our model predicts that the crossover between the power law regime with $\beta=2$ ($Z=3$) and the plateau of the experimental distribution of Δt scales with M as $1/2^M$. Using this prediction, we estimate M from the experimental data as $M\approx14$ for the spike detection threshold of 1% and $M\approx10$ for the threshold of 8%. The two curves for different thresholds collapse after scaling them with the corresponding values of M [Fig. 12(b)].
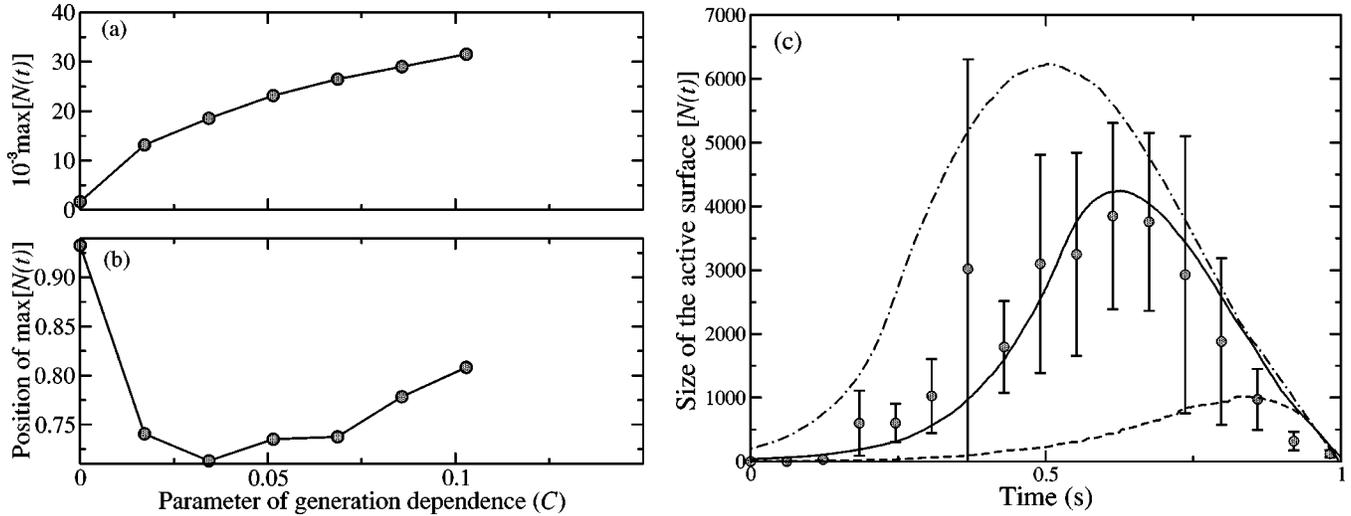
FIG. 13. Active surface features and experimental active surface. Value of the maximum size (a) and peak position (b), of the active surface vs the parameter C describing generation dependence [Eq. (2)]. (c) Experimental and predicted active surfaces. Circles with error bars are the experimental active surfaces obtained from 12 distinct inflations from the collapsed state. The dashed line is the active surface when a random opening pressure threshold is applied, the solid line is obtained with a small generation dependence $C=0.01$, and the dot-dash line corresponds to a strong generation dependence $C=0.02$. In all simulated results, we used a symmetric tree with 15 generations averaged over 1000 realizations.

VI. DISCUSSION

Power law behavior is usually interpreted as a fractal or scale-free phenomenon, implying the absence of a characteristic scale. Here, we examined the time intervals Δt between consecutive crackles during lung inflation and find that the distribution of Δt follows a power law with exponent $\beta \approx 2$. To study the microscopic origins of the scaling behavior, we used a dynamic invasion percolation model of avalanches in a Cayley tree [27]. The exponent β of the power law distribution is robust under different distributions of the pressure threshold, as well as the asymmetry and coordination number $Z>2$ of the tree structure. For a linear chain $Z=2$, the distribution of time intervals Δt is similar to the distribution of waiting times in a Poisson process of queuing and consequently, the exponent of the distribution is $\beta=1$ [57].

Power law distributions, however, do not always provide information about the microscopic dynamics of the process. Thus, to explore the microscopic dynamics of the system, we introduce the concept of an active surface that consists of the branches that are closed but connected to the root of the tree by an open pathway. Initially, the size of the active surface increases exponentially as the opening of a single branch on the active surface adds $(Z-1)$ new branches, increasing the size by $(Z-2)$. However, when an avalanche reaches the boundary of the tree, the size of the active surface decreases, becoming zero when all branches are open. The maximum size of the active surface and the pressure at that point characterize the dynamics of the opening process. We find that, in contrast to the distribution of Δt, the active surface is sensitive to the properties of the tree structure as well as to the dynamic mechanisms of the opening process.

For completely random opening pressure thresholds, the evolution of the active surface is given by Eq. (32). The

position of the peak is $P_{max} \approx (1-1/M)$. In the limit when every generation has the same deterministic opening pressure threshold which is greater than that of its parent, branches within the same generation open simultaneously. The corresponding active surface grows in geometric steps with a factor of $(Z-1)$ until the last generation opens. When the last generation opens, the size of the active surface drops to zero. As the distribution of pressure thresholds becomes more and more generation dependent, the height and width of the peak monotonically increases (see Fig. 13). With increasing C in Eq. (2), the position of the peak of the active surface initially shifts towards lower pressures, until the pressure threshold distributions of the individual generations cease to overlap (see Fig. 3). Further increasing C, the peak of the active surface starts to shift towards higher pressures (see Fig. 13).

An asymmetric tree has some alveoli which are closer to the top of the tree while others are father away. The alveoli which are closer to the top are more likely to open at lower pressures than those that are deeper into the tree [46]. We note that the size of the active surface decreases only when an opening sequence reaches the alveoli. Thus, in an asymmetric tree, the size of the active surface is smaller at the beginning of inflation than in a symmetric tree with the same number of branches. However, since an equal number of alveoli opens at higher pressures, the position and height of the peak remain almost the same, but the width of the peak decreases (see Fig. 5).

For a linear chain, the active surface can at most consist of a single branch. With an increasing coordination number $(Z>2)$, the position of the peak remains the same [$P_{max} \approx (1-1/M)$], while the height increases as $N_{max} \propto (Z-1)^{M-1}$ [see Eq. (33)].

With regard to physiological implications, we suggest that it is possible to reconstruct the evolution of the active surface

from experimental data on crackle sounds using the relation between the average size of the active surface and the average time interval among crackles. For this purpose, we calculate the average time interval between measured crackles in a nonoverlapping moving time window and obtain the average size of the active surface using Eq. (25). The active surfaces thus reconstructed are averaged over data from 12 different inflations. The results, shown in Fig. 13, suggest that the opening pressure thresholds have a weak generation dependence in the lung. Additionally, we assumed in this study that the speed of the avalanche is infinity, which is reasonable for the range of Δt we investigate here. In previous study, the importance of finite avalanche speed has been investigated [9]. When the inflation rate becomes comparable to the avalanche speed, the overlap of avalanches may lead to new phenomena such as instabilities and negative stiffness [29].

We conclude that the slope β of the distribution of Δt for a Cayley tree is mainly due to the branching hierarchical structure. From the mean field calculation, we find that detectable crackles come from the last 14 generations after the first closed airway in the lobe. The agreement of the model with experimental data is consistent with the possibility that in the 14 generations of the airway tree from which we can detect crackles, the distributions of opening threshold pressures from different generations overlap significantly so as to allow avalanchelike opening of airways. Our findings also have a potential clinical application. While the distribution of Δt can be used to estimate the accuracy of crackle sound detection, the dynamic active surface may provide information about the generation dependence of pressure thresholds, which in turn may be characteristic of various lung diseases.

ACKNOWLEDGMENT

[1] J.P. Sethna, K.A. Dahmen, and C.R. Myers, Nature (London) **410**, 242 (2001).

[2] B. Gutenberg and C.F. Richter, *Seismicity of the Earth* (Princeton University Press, Princeton, 1949).

[3] J.P. Sethna, K. Dahmen, S. Kartha, J.A. Krumhansl, B.W. Roberts, and J.D. Shore, Phys. Rev. Lett. **70**, 3347 (1993).

[4] E.M. Kramer and A.E. Lobkovsky, Phys. Rev. E **53**, 1465 (1996).

[5] L.I. Salminen, A.I. Tolvanen, and M.J. Alava, Phys. Rev. Lett. **89**, 185503 (2002).

[6] R.T.H. Laënnec, *De l'ausculation Médiate ou Traitédu Diagnostic des Maladies des Poumons et du Coeur, Fondé Principalement sur ce Nouveau Moyen D'exploration* (Brosson et Chaudé, Paris, 1819).

[7] H. Pasterkamp, S.S. Kraman, and G.R. Wodicka, Am. J. Respir. Crit. Care Med. **156**, 974 (1997).

[8] J.B. Grotberg, Annu. Rev. Biomed. Eng. **3**, 421 (2001).

[9] A.M. Alencar, S.V. Buldyrev, A. Majumdar, H.E. Stanley, and B. Suki, Phys. Rev. Lett. **87**, 088101 (2001).

[10] A.M. Alencar, Z. Hantos, F. Peták, J. Tolnai, T. Asztalos, S. Zapperi, J.S. Andrade, Jr., S.V. Buldyrev, H.E. Stanley, and B. Suki, Phys. Rev. E **60**, 4659 (1999).

[11] R.L.H. Murphy, Jr., S.K. Holford, and W.C. Knowler, N. Engl. J. Med. **296**, 968 (1977).

[12] A.R. Nath and L.H. Capel, Thorax **35**, 694 (1980).

[13] R.L.H. Murphy, Jr., A. Gaensler, S.K. Holford, E.A. Del-Bono, and G. Epler, Am. Rev. Respir. Dis. **129**, 375 (1984).

[14] P. Piirilä, A.R.A. Sovijärvi, T. Kaisla, H.M. Rajala, and T. Katila, Chest **99**, 1076 (1991).

[15] Y. Ploysongsang, R.P. Michel, A. Rossi, L. Zocchi, J. Milic-Emili, and N.C. Staub, J. Appl. Physiol. **66**, 2061 (1989).

[16] N. Al-Jarad, B. Strickland, S. Lock, R. Logan-Sinclair, and R.M. Rudd, Thorax **48**, 347 (1993).

[17] N. Al-Jarad, S.W. Davies, R. Logan-Sinclair, and R.M. Rudd, Respir. Med. **88**, 37 (1994).

[18] A.R.A. Sovijärvi, P. Pirilä, and R. Luukkonen, Clin. Physiol. **16**, 172 (1996).

[19] E.R. Weibel, *Morfometry of the Human Lung* (Academic, New York, 1963).

[20] M.F. Shlesinger and B.J. West, Phys. Rev. Lett. **67**, 2106 (1991).

[21] K. Horsfield, W. Kemp, and S. Phillips, J. Appl. Physiol.: Respir., Environ. Exercise Physiol. **52**, 21 (1982).

[22] J.S. Andrade, Jr., A.M. Alencar, M.P. Almeida, J. Mendes Filho, S.V. Buldyrev, S. Zapperi, H.E. Stanley, and B. Suki, Phys. Rev. Lett. **81**, 926 (1998).

[23] R.D. Kamm and R.C. Schroter, Respir. Physiol. **75**, 141 (1989).

[24] M. Heil and J.P. White, J. Fluid Mech. **462**, 79 (2002).

[25] R.G. Crystal, J.B. West, E.R. Weibel, and P.J. Barnes, *The Lung: Scientific Foundations* (Lippincott-Raven, Philadelphia, 1997).

[26] B. Suki, A.L. Barabási, Z. Hantos, F. Peták, and H.E. Stanley, Nature (London) **368**, 615 (1994).

[27] A.-L. Barabási, S.V. Buldyrev, H.E. Stanley, and B. Suki, Phys. Rev. Lett. **76**, 2192 (1996).

[28] B. Suki, A.M. Alencar, J. Tolnai, T. Asztalos, F. Peták, M.K. Sujeer, K. Patel, J. Patel, H.E. Stanley, and Z. Hantos, J. Appl. Physiol. **89**, 2030 (2000).

[29] A.M. Alencar, S. Arold, S.V. Buldyrev, A. Majumdar, D. Stamenović, H.E. Stanley, and B. Suki, Nature (London) **417**, 809 (2002).

[30] J.R. Claycomb, K.E. Bassler, J.H. Miller, M. Nersesyan, and D. Luss, Phys. Rev. Lett. **87**, 178303 (2001).

[31] O. Perkovic, K. Dahmen, and J.P. Sethna, Phys. Rev. Lett. **75**, 4528 (1995).

[32] G. Durin and S. Zapperi, Phys. Rev. Lett. **84**, 4705 (2000).

[33] N. Vandewalle, J.F. Lentz, S. Dorbolo, and F. Brisbois, Phys. Rev. Lett. **86**, 179 (2001).

[34] P.J. Cote and L.V. Meisel, Phys. Rev. Lett. **67**, 1334 (1991).

[35] C.W. Eurich, J.M. Herrmann, and U.A. Ernst, Phys. Rev. E **66**, 066137 (2002).

[36] M. Kardar, G. Parisi, and Y.C. Zhang, Phys. Rev. Lett. **56**, 889 (1986).

[37] T. Poinsot, D. Veynante, and S. Candel, J. Fluid Mech. **228**, 561 (1991).

[38] P. Raybaud, J. Hafner, G. Kresse, and H. Toulhoat, Phys. Rev. Lett. **80**, 1481 (1998).

[39] A.M. Alencar, J.S. Andrade, Jr., and L.S. Lucena, Phys. Rev. E **56**, R2379 (1997).

[40] D. Ben-Avraham and S. Havlin, *Diffusion and Reactions in Fractals and Disordered Systems* (Cambridge University Press, Cambridge, 2000).

[41] P. Leblanc, F. Ruff, and J. Milic-Emili, J. Astrophys. Astron. **28**, 448 (1970).

[42] D.I.M. Siegler and Y.F.L.A. Engel, Am. Rev. Respir. Dis. **114**, 123 (1976).

[43] R.S. Tepper, S.J. Gunst, C. Doerschuk, X. Shen, and W. Bray, J. Appl. Physiol. **78**, 505 (1995).

[44] D.P. Gaver, III, R.W. Samsel, and J. Solway, J. Appl. Physiol. **69**, 74 (1990).

[45] E.T. Naureckas, C.A. Dawson, B. Gerber, D.P. Gaver, III, H.L. Gerber, J.H. Linehan, J. Solway, and R.W. Samsel, J. Appl. Physiol. **76**, 1372 (1994).

[46] A. Majumdar, A.M. Alencar, S.V. Buldyrev, Z. Hantos, H.E. Stanley, and B. Suki, Phys. Rev. Lett. **87**, 058102 (2001).

[47] A. Majumdar, A.M. Alencar, S.V. Buldyrev, Z. Hantos, H.E. Stanley, and B. Suki, Phys. Rev. E **67**, 031912 (2003).

[48] D. Halpern and J.B. Grotberg, J. Fluid Mech. **237**, 1 (1992).

[49] O.E. Jensen and J.B. Grotberg, J. Fluid Mech. **240**, 259 (1992).

[50] P.D. Howell, S.L. Waters, and J.B. Grotberg, J. Fluid Mech. **406**, 309 (2000).

[51] H. Kitaoka and B. Suki, J. Appl. Physiol. **82**, 968 (1997).

[52] O.E. Jensen, Phys. Fluids **6**, 1084 (1994).

[53] K. Horsfield, G. Dart, and D.E. Olson, J. Appl. Physiol. **31**, 207 (1971).

[54] J.M. Harris, J.L. Hirst, and M.J. Mossinghoff, *Combinatorics and Graph Theory* (Springer, New York, 2000).

[55] P.J. Cameron, *Combinatorics: Topics, Techniques and Algorithms* (Cambridge University Press, Cambridge, 1994).

[56] *Handbook of Mathematical Functions, With Formulas, Graphs, and Mathematical Tables* edited by M. Abramowitz and I.A. Stegun (Dover, New York, 1974).

[57] H.A. Taha, *Operations Research: An Introduction* (Macmillan, New York, 1992).

[58] C. Derman, L.J. Gleser, and I. Olkin, *A Guide to Probability Theory and Application* (Holt, Reinhart and Winston, New York, 1973).

[59] S.M. Ross, *Introduction to Probability Models* (Academic, New York, 1997).

[60] For the lung, the only realistic structure is when $Z=3$. The reason to explore different Z values is to determine the effects of the tree structure on the power law distribution of time intervals we experimentally measure.

[61] An airway either branches into $(Z-1)$ daughters, or terminates into an air sac. A daughter (i',j') of a parent airway (i,j) is given by $(i',j')\equiv[i+1,(Z-1)j+x]$, where $x\in[0,(Z-1)]$. Branches which terminate in an air sac are the terminal branches of the airway tree.